PAPER

Ab initio multiple spawning on laser-dressed states: a study of 1,3-cyclohexadiene photoisomerization via light-induced conical intersections

IOP Publishing Journal of Physics B: Atomic, Molecular and Optical Physics
J. Phys. B: At. Mol. Opt. Phys. **48** (2015) 164003 (10pp) doi:10.1088/0953-4075/48/16/164003

Ab initio multiple spawning on laser-dressed states: a study of 1,3-cyclohexadiene photoisomerization via light-induced conical intersections

Jaehee Kim, Hongli Tao, Todd J Martinez and Phil Bucksbaum

PULSE Institute, Stanford University, Stanford, CA 94304, USA

E-mail: jk2236@stanford.edu

Received 14 April 2015, revised 9 June 2015
Accepted for publication 12 June 2015
Published 15 July 2015

Abstract

We extend the *ab initio* multiple spawning method to include both field-free and field-induced nonadiabatic transitions. We apply this method to describe ultrafast pump-probe experiments of the photoinduced ring-opening of gas phase 1,3-cyclohexadiene. In the absence of a control field, nonadiabatic transitions mediated by a conical intersection (CoIn) lead to rapid ground state recovery with both 1,3-cyclohexadiene and ring-opened hexatriene products. However, application of a control field within the first 200 fs after photoexcitation results in suppression of the hexatriene product. We demonstrate that this is a consequence of population dumping prior to reaching the CoIn and further interpret this in terms of light-induced CoIns created by the control field.

Keywords: *ab initio* multiple spawning, light induced conical intersections, coherent control, photoisomerization, 1,3-cyclohexadiene

(Some figures may appear in colour only in the online journal)

1. Introduction

Strong electric fields are a powerful tool for controlling atomic and molecular dynamics. By altering the potential energy surface (PES) topography in atoms and molecules, strong fields can open reaction channels that are otherwise inaccessible. Much work has been done with this control method in atoms and diatomic molecules, where the non-adiabatic dynamics take place at avoided crossings [1–6]. We have expanded this idea to molecular systems where conical intersections (CoIns), i.e. true crossings of adiabatic PESs, play an important role in the nonadiabatic dynamics.

Our model system, 1,3-cyclohexadiene (CHD), is a prototypical photochemical electrocyclic reaction through a CoIn. It has been studied extensively both theoretically and experimentally [7–25]. Upon photoexcitation to the bright 1B state by ultraviolet (UV) light, the excited state wavepacket rapidly crosses onto the 2A state where it continues to evolve to the 1A ground state. At the 2A/1A CoIn, the wavepacket bifurcates. Approximately half of the population returns back to the CHD geometry and the other half proceeds along the ring-opening reaction coordinate to form all-cis-Hexatriene (HT) [24–26]. This isomerization is the result of wavepacket propagation through (or near) one or more CoIns.

Most previous studies of methods to control the quantum dynamics of CHD isomerization have focused on shaping the initial wavepacket [22–24, 27–29]. An alternative approach employs a control field to alter dynamics at or before the CoIn. Recent experiments have demonstrated effective control using control laser fields that can influence the PES topography and wave packet dynamics in the vicinity of the CoIn [30]. The control field dresses the molecule, creating an effective ring of resonance around the CoIn that can be viewed as the locus of light-induced conical intersections (LICI) [31].

Experiments have concluded that a LICI can efficiently suppress HT production [30]. To demonstrate this, a UV pump pulse is followed by a strong field 800 nm pulse at a

variable time delay. Long after the excited state dynamics are completed, an intense fragmentation pulse probes the final state at a set time delay from the pump. The fragmented ions are collected by time of flight (TOF) mass spectrometry. Principal component analysis [32] is used to extract the control field effect from the acquired TOF spectra.

To provide a detailed molecular explanation of this experiment, we performed a quantum molecular dynamics simulation on the excited state of laser-dressed CHD in the gas phase. There have been several techniques incorporating laser fields into the quantum–classical dynamics based on trajectory surface hopping methodology [33–37], most notably the 'field-induced surface-hopping' (FISH) [38–42] and 'surface hopping in adiabatic representation including arbitrary couplings' (SHARC) [43–46] methods. In this work, we used the extended *ab initio* multiple spawning (AIMS) method to include both field-free and field-induced nonadiabatic couplings. Since the AIMS method is fully quantum mechanical, one can expect that it will be able to describe coherence phenomena more accurately than surface-hopping type methods. Previous work using AIMS has included field-free or field-induced couplings [47, 48], but not both simultaneously. We further extend the formalism for field-induced nonadiabatic couplings to include an arbitrary number of photon-dressed electronic states.

Our calculations predict that more than 90% of the excited state population passes through the CoIn in the absence of the control field. However, in the presence of the control field, the excited state wavepacket is efficiently transferred to the ground state by the control field near the LICI, before it reaches the CoIn. The result is suppression of HT production. We can understand this suppression by incorporating a control field into the field-free molecular Hamiltonian. This transition occurs when the wavepacket meets the 800 nm 'quantum resonance ring'. Each point on the QRR is a dressed state crossing, where a LICI is located.

2. Theory

2.1. Overview of AIMS

The details of AIMS can be found elsewhere [48–54]. Here, we give only a brief introduction. In AIMS, the nuclear and electronic Schrödinger equations are solved simultaneously and the local PES, gradient, electronic wavefunction and nonadiabatic couplings are evaluated numerically on the fly, as needed by the dynamics. The AIMS wavefunction ansatz is a superposition of products of nuclear and electronic wavefunctions. Each nuclear wavefunction associated with each electronic state is expressed as a linear combination of time-dependent frozen Gaussian basis functions, i.e. trajectory basis functions (TBFs) centered at the classical position and momentum in phase space with the full dimensionality of the system under investigation. The center of each TBF propagates according to classical equations of motion on a single adiabatic electronic state and the time evolution of complex coefficients associated with the TBFs is governed by the nuclear Schrödinger equation. When a TBF enters a region with high nonadiabatic coupling, a new TBF is 'spawned'. The spawned function enters the simulation with a vanishing amplitude and is only populated through the solution of the nuclear Schrödinger equation. AIMS can simulate quantum dynamics without a priori knowledge of the global PES, and also in the presence of large nonadiabatic couplings where the Born–Oppenheimer approximation breaks down. The full-dimensional PES is calculated as needed, thereby eliminating uncertainties that arise when restricting the dynamics to one or a few reaction coordinates. In this work, we use AIMS as implemented in the MOLPRO quantum chemistry package [52, 55].

2.2. Detailed formalism for photon field

The dressed states can be viewed in a Floquet picture with energies shifted from the nondressed states by integer multiples of the photon energy [31, 56–59]. New CoIns form when dressed states with different photon indices intersect with the original states. The two-dimensional subspace of the LICI is defined by basis vectors along the energy difference gradient and the dipole coupling gradient in the dressed state space. We describe the molecule–light interaction within the dipole approximation in our work. The characteristics of LICIs can be controlled by varying the laser field frequency and intensity. The frequency of the laser field dictates the location of the LICI with respect to the energy difference between coupled states, and the energy difference gradient and transition dipole moment vectors determine the two-dimensional subspace of the LICI, analogous to the energy difference gradient and nonadiabatic coupling vectors which determine the space of a CoIn formed by the Born–Oppenheimer surfaces. For standard CoIns, nonadiabatic couplings between two electronic states trigger the spawning. To account for the population transfer through LICI, we monitor the molecule–light interaction (dipole coupling term) which is the off-diagonal (in the photon index) term in the Hamiltonian between dressed states.

We assume an oscillating control field with a slowly varying envelope: $\vec{E}(t) = \hat{\varepsilon}E_0(t)\cos(\omega t)$. In this case we can modify the AIMS equations to incorporate the Floquet ansatz, which states that an interaction Hamiltonian that is strictly periodic in time with period $2\pi/\omega$ must give rise to solutions that can be expressed as a Fourier series in $n\omega t$ [57–62]. The modified wavefunction ansatz becomes:

$$|\,|\psi(\mathbf{r},\mathbf{R},t)\rangle\rangle = \sum_I \sum_i \sum_n c_i^{I,n}(t)\left|\chi_i^{I,n}(\mathbf{R},t)\phi^{I,n}(\mathbf{r};R)\right\rangle \otimes |\,n;\omega\rangle, \quad (1)$$

where $\phi^{I,n}$ is the electronic wavefunction of state I dressed by n photons, $\chi_i^{I,n}$ is the ith time-dependent TBF associated with $\phi^{I,n}$, $c_i^{I,n}$ is the complex amplitude of the TBF $\chi_i^{I,n}$, **r**/**R** denote the electronic/nuclear coordinates, and $|\,n;\omega\rangle$ is an eigenstate of the relative photon number operator, N_r, with eigenvalue $n\omega$ [62–64]. The individual terms in this series are 'dressed states', which contain an additional index n (the

photon index or Floquet index) along with additional time dependence $e^{in\omega t}$. The Hamiltonian can be divided into three parts corresponding to the light field, the molecule, and the light–matter interaction. Using the dipole approximation for the light–matter interaction, the Hamiltonian becomes:

$$\begin{aligned} H_{\text{total}} &= H_{\text{light}} + H_{\text{molecule}} + H_{\text{interaction}} \\ &= N_r + H_{\text{molecule}} - \vec{\mu} \cdot \vec{E}(t). \end{aligned} \tag{2}$$

Using the wavefunction ansatz in equation (1) and the Hamiltonian of equation (2), the time-dependent Schrödinger equation becomes:

$$\begin{aligned} &\sum_{I,i,n} \dot{c}_i^{I,n}(t) \left|\chi_i^{I,n}(\mathbf{R}, t)\phi^{I,n}(\mathbf{r}; \mathbf{R})\right\rangle \otimes |n; \omega\rangle \\ &\quad + \sum_{I,i,n} c_i^{I,n}(t) \frac{\partial}{\partial t} \left|\chi_i^{I,n}(\mathbf{R}, t)\phi^{I,n}(\mathbf{r}; \mathbf{R})\right\rangle \otimes |n; \omega\rangle \\ &\quad = \left[N_r + H_{\text{molecule}} - \vec{\mu} \cdot \vec{E}(t)\right] \\ &\quad \times \left|\chi_i^{I,n}(\mathbf{R}, t)\phi^{I,n}(\mathbf{r}; \mathbf{R})\right\rangle \otimes |n; \omega\rangle. \end{aligned} \tag{3}$$

Multiplying both sides by $\left\langle \chi_j^{J,m}\phi^{J,m}\right| \otimes \langle m; \omega|$, using the rotating wave and slowly varying envelope approximations and simplifying gives:

$$\begin{aligned} &\mathrm{i}\sum_j S_{kj}^{J,m;J,m}\dot{c}_j^{J,m} = \sum_{I,j} H_{kj}^{J,m;I,m} c_j^{I,m} \\ &\quad - \sum_{I\neq J,j} \left(S_{kj}^{J,m;I,m+1} c_j^{I,m+1} + S_{kj}^{J,m;I,m-1} c_j^{I,m-1}\right) \\ &\quad \times \vec{\mu}^{JI} \cdot \hat{\varepsilon} E_0(t) - \sum_j \left(\mathrm{i}\dot{S}_{kj}^{J,m;J,m} - m\omega S_{kj}^{J,m;J,m}\right) c_j^{J,m}, \end{aligned} \tag{4}$$

where the overlap matrix is defined as $S_{ij}^{I,n;J,m} = \left\langle \chi_i^{I,n} | \chi_j^{J,m} \right\rangle_R$, it's time dependence is represented by $\dot{S}_{ij}^{I,n;J,m} = \left\langle \chi_i^{I,n} | \frac{\partial}{\partial t} \chi_j^{J,m} \right\rangle_R$, the transition dipole matrix element between the Ith and Jth electronic states is $\vec{\mu}^{JI}$, and the matrix elements of the molecular Hamiltonian are $H_{ij}^{I,n;J,m} = \left\langle \chi_i^{I,n}\phi^{I,n}\right| H_{\text{molecule}} \left|\chi_j^{J,m}\phi^{J,m}\right\rangle_{R,r}$. We suppress from this expression the overall state-independent contribution to the total energy that comes from the laser field. The first term on the right-hand side describes the usual AIMS formalism where population transfer occurs via nonadiabatic coupling. The second term on the right-hand side represents the light–matter interaction term. We collect these terms into a new effective Hamiltonian matrix $\tilde{H}$ as follows:

$$\tilde{H}_{ij}^{I,n;I,m} = \left(H_{ij}^{I,n;I,m} + n\omega S_{ij}^{I,n;I,m}\right)\delta_{nm}, \tag{5}$$

$$\begin{aligned} \tilde{H}_{ij}^{I,n;J,m} &= H_{ij}^{I,n;J,m}\delta_{nm} - \left(S_{ij}^{I,n;J,m}\delta_{n+1,m}\right. \\ &\quad \left. + S_{ij}^{I,n;J,m}\delta_{n-1,m}\right)\vec{\mu}^{IJ} \cdot \hat{\varepsilon} E_0(t). \end{aligned} \tag{6}$$

The diagonal terms in equation (5) represent the energy of the dressed states, including both the energy of the molecule and photon. The TDSE simplifies to:

$$\begin{aligned} &\mathrm{i}\sum_j S_{kj}^{J,m;J,m}\dot{c}_j^{J,m} \\ &\quad = \sum_j \left[\left(\tilde{H}_{kj}^{J,m;J,m} - \mathrm{i}\dot{S}_{kj}^{J,m;J,m}\right)c_j^{J,m} + \sum_{I\neq J,n} \tilde{H}_{kj}^{J,m;I,n} c_j^{I,n}\right]. \end{aligned} \tag{7}$$

Each TBF propagates on a given dressed electronic state and the time-dependent complex coefficients of the TBFs are determined by solving the TDSE in this basis set through equation (7). In this formalism, there are two classes of CoIns. The first class involves degeneracies between two different electronic states with the same photon index. This is the original CoIn where nonadiabatic transitions occur. The second class involves degeneracies between two states with different photon indices, which we call LICIs. New TBFs are spawned when the off-diagonal coupling term in the effective Hamiltonian is large. This can occur either when the nonadiabatic coupling term is large (above a set threshold), describing a standard CoIn, or also when the dipole coupling term is large, describing the effect of a LICI.

3. Applications

3.1. Test case

Before applying our new formulation to a multi-dimensional case, we tested our formalism with low-dimensional two-state model systems and compare them against their numerically exact solutions. For the numerically exact solution, the time dependent Schrödinger equation was propagated on a grid using the Newton polynomial propagation scheme [65] with a time step of 10 atomic time units. The grid used contains 1024 points for the one dimensional system and is a rectilinear direct product with 256 points in each dimension for the two dimensional system. The time-dependent Schrödinger equation that is solved on the grid may be written as:

$$\mathrm{i}\begin{pmatrix} \dfrac{\partial\psi_g}{\partial t} \\ \dfrac{\partial\psi_e}{\partial t} \end{pmatrix} = \begin{pmatrix} T_g + V_g & \mu E_0(t) \\ \mu E_0(t) & T_e + V_e \end{pmatrix}\begin{pmatrix} \psi_g \\ \psi_e \end{pmatrix}. \tag{8}$$

The envelope of the laser pulse is Gaussian with the form

$$E_0(t) = A\mathrm{e}^{-\frac{2\log 2\left(t-t_{\text{pulse}}\right)^2}{t_{\text{duration}}^2}} \tag{9}$$

centered at $t_{\text{pulse}} = 60$ fs with FWHM $t_{\text{duration}} = 30$ fs and amplitude 0.00193 au or 0.00386 au. The direction of the electric field was chosen to be parallel to the transition dipole moment at all times and the magnitude of the transition dipole moment was kept as a constant at 0.181 au.

For the one dimensional test case, we used the two lowest states of the iodine molecule (figure 1) represented by Morse

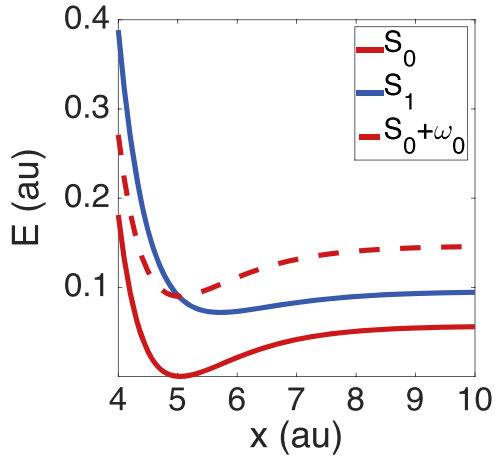

Figure 1. Potential energy curves for the one dimensional test case. The ground state is dressed by an external laser pulse (dotted red line).

potentials with parameters defined in table 1.

$$V_{g/e} = D_{g/e}\left(1 - \mathrm{e}^{-b_{g/e}(x-x_{re,g/e})}\right)^2 + T_{g/e}. \tag{10}$$

The laser frequency is tuned to 0.089868 au to maximize the absorption probability between the Franck–Condon (FC) and laser induced CoIn. Once the ground state population is initialized, the spawning occurs immediately due to the proximity of the light induced crossing to the FC point (figure 2). New trajectories were spawned every ten time steps per coupling event, in analogy with the continuous spawning introduced previously [66]. The new spawned basis function had the same momentum as its parents and was propagated in the diabatic representation. By the end of the simulation, ~7% of the ground state population was transferred to the excited state at a field strength 0.00193 au and ~25% at 0.00386 au. For both field strengths, the numerically exact method and AIMS gave very similar results (figure 3).

We then extended our test to a two dimensional model system. The PES in this case is a product of two independent one-dimensional functions: a Morse potential in one dimension (denoted x) with the same parameters as in our 1D test case, and a harmonic potential in the other dimension (denoted y). The harmonic potential shared the same center as the Morse potential at 5.0386 au with force constant 0.16 au.

The results from our AIMS method agree closely with the numerically exact results in the two-dimensional case (figures 4 and 5). Once the wavefunction is launched on the excited state via the LICI, it continues to grow for the first 80 fs, after which it starts moving in the x-direction under the influence of the PES gradient. The wavefunction reaches its classical turning point in x at 160 fs.

Both of these tests of our new formulation on the low-dimensional model system yielded agreement with exact numerical results for both population transfer as well as nuclear wavefunction propagation. This gives us confidence to apply our new formalism to a real system, the CHD ring opening reaction.

3.2. CHD

AIMS-CASSCF was used with an active space consisting of six electrons in four orbitals for the electronic structure, averaging over three states SA-3-CAS(6/4) with the 6–31 G* basis set. The details of the active space choice were discussed in our previous work [26]. We initialized 20 simulations at the FC region on S_1, sampling the initial positions and momenta from a Wigner distribution corresponding to the ground vibrational state (in a harmonic approximation). The central geometry and harmonic frequencies came from ground state (S_0) optimization using MP2/6–31 G*. Spawning was triggered when either the norm of the nonadiabatic coupling vector was larger than a preset spawning threshold (20.0 au) or when the coupling due to the laser field exceeded 4.0 au. After 500 fs, 175 trajectories were generated through the spawning procedure. For each of the 20 simulations, we started with an external laser field at various delays, with intervals of 10 fs, provided that there was still population left on the excited state. The envelope of the external laser field is described by a Gaussian function in the time domain:

$$E_0(t) = \hat{\varepsilon} E_{\mathrm{Amp}} \mathrm{e}^{-\frac{2\log 2 (t-t_0)^2}{E^2_{\mathrm{duration}}}}. \tag{11}$$

Upon excitation by the UV pump, the molecules are selectively excited via dipole selection rule at the FC geometry. Since the molecule has C_2 symmetry at the FC geometry, only μ_x and μ_y are allowed for the S_0–S_1 (1A–1B) transition. Our calculation estimated that, at the FC geometry, $(\mu_x, \mu_y, \mu_z) = (-0.269, 1.526, -0.057)$ au, so most of the excited state population to S_1 (1B) state will be aligned in the y-direction. The spectroscopic axes of CHD at FC geometry are shown in figure 6. In reality, the geometric alignment will have a $\cos^2\theta$ distribution but our simulation models are idealized case where this distribution is infinitely narrow. In the experiment, the IR control field was parallel to the UV pump pulse. Assuming the initial UV excitation freezes the molecular frame axis via geometric alignment and the molecule does not rotate within our simulation time scale, we can approximately define the polarization of the IR control field ($\hat{\varepsilon}$) in the molecular frame. To simulate the experimental results [30], we chose laser parameters mimicking those used in our experiment; the intensity of the laser is 0.04 au (2.31×10^{10} V m^{-1}) and E_{duration} is ~70 fs to fit the FWHM of the external control laser field. The UV-pump/IR-control delay time t_0 was varied from 0 to 200 fs in steps of 10 fs. Each simulation was run for 200 fs and at the end of the simulation, the TBFs transferred to the ground state by the control field were analyzed to determine their end product, CHD or HT. After TBFs were transferred to the S_0 surface, we switched to ground state dynamics (no longer allowing nonadiabatic transitions nor solving for the excited electronic state PESs) and followed the TBF until the final product (HT or CHD) could be identified.

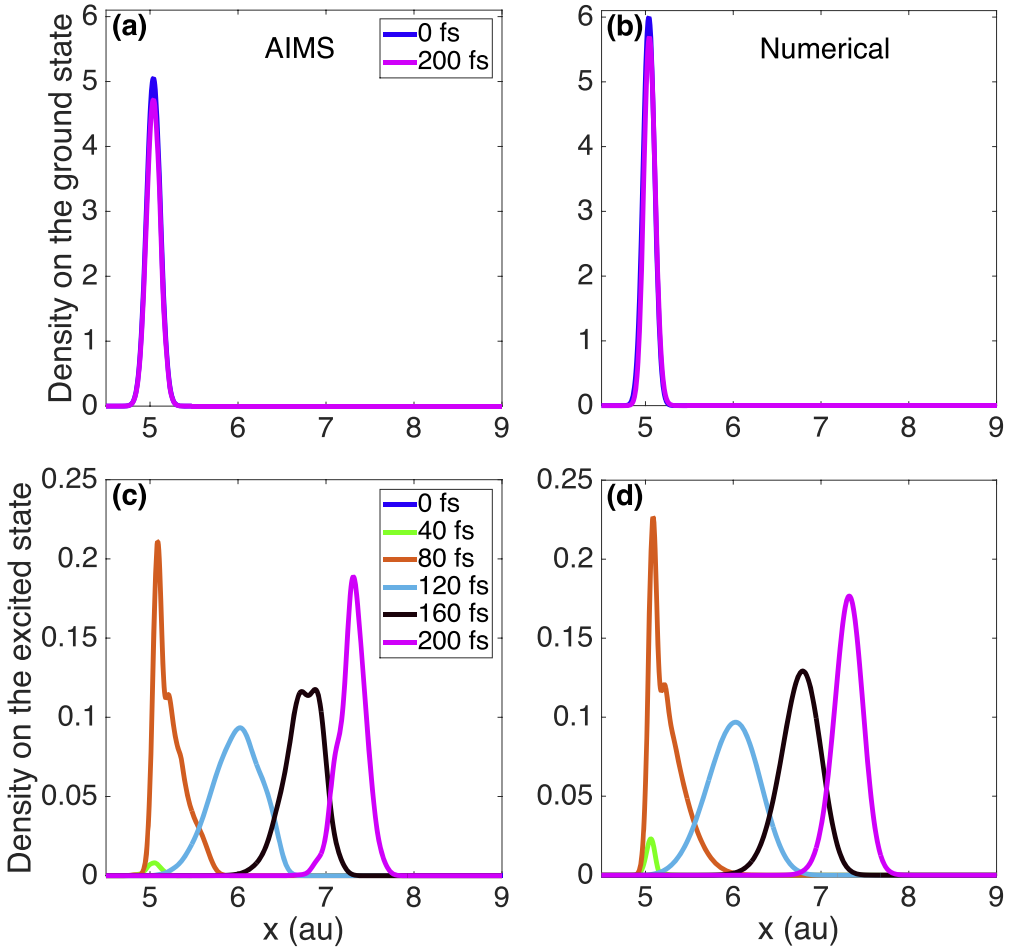

Figure 2. Wavefunction in the ground and excited states at various times during a photo-absorption process for the one-dimensional model system.

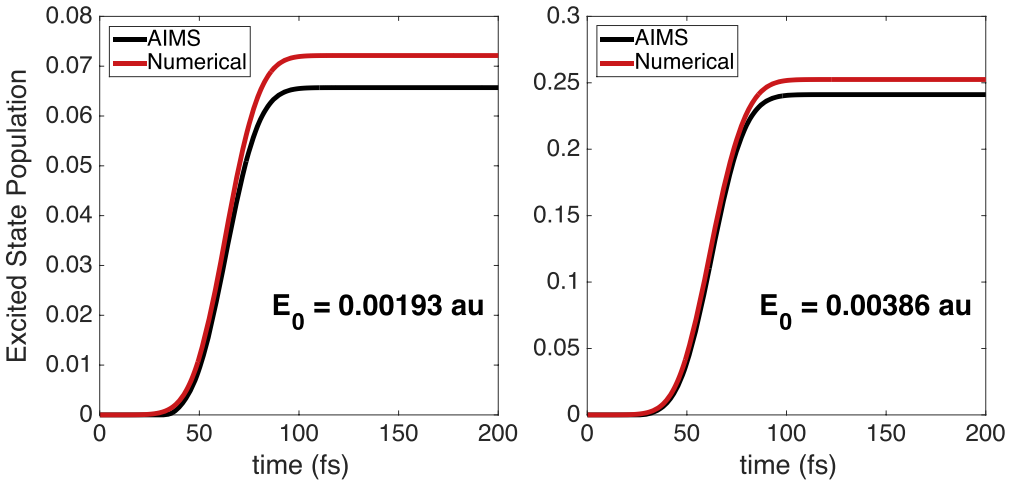

Figure 3. Population transfer during a photo-absorption process for the one-dimensional model system at two different field strengths.

4. Results and discussion

We attribute the nature of our control result to the QRR/LICI, a closed loop that encloses the CoIn and consists of points where two surfaces (S_1/S_0) are resonant in the presence of 800 nm light. In figure 7, we plot the QRR in the S_1/S_0 branching plane spanned by two internal vector coordinates g and h, where g is the energy difference gradient vector and h is the nonadiabatic coupling vector [67–70]. The degeneracy is lifted linearly with displacement within the branching plane near the CoIn. In a dressed state picture, every point in the QRR is a point of degeneracy between dressed states with

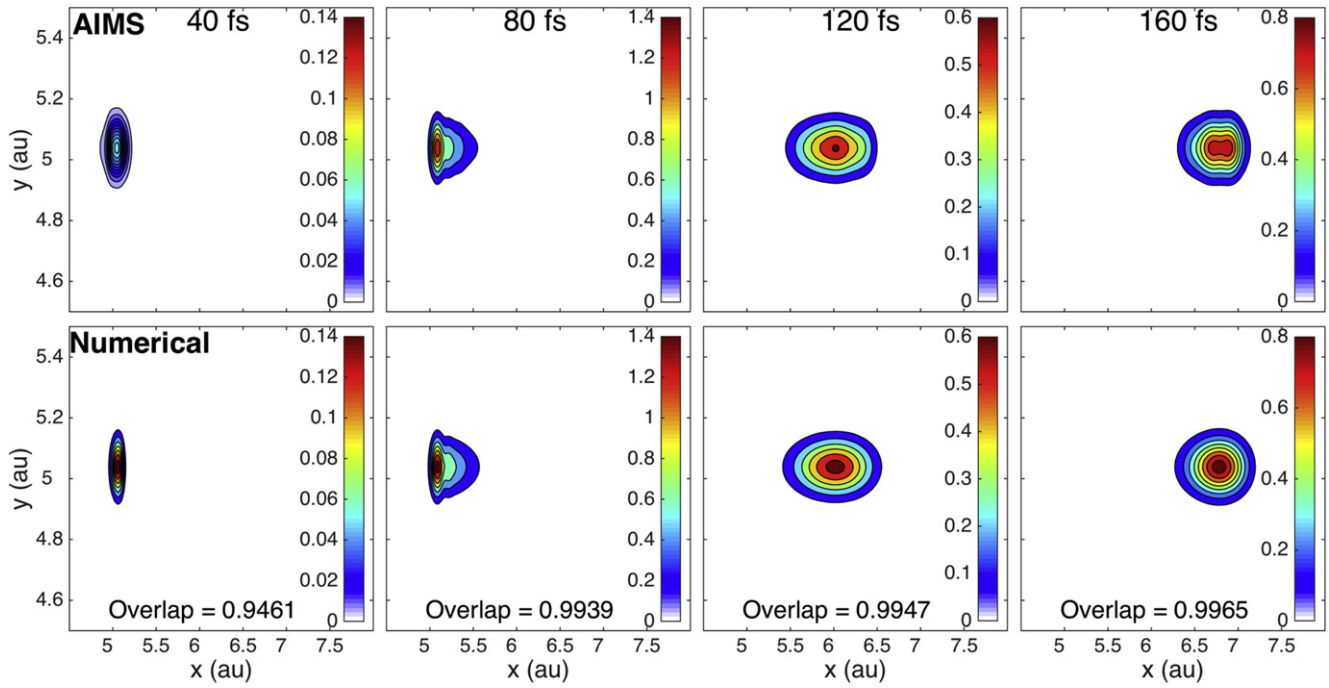

Figure 4. Comparison of the probability density on the exited state at various time delays for the two-dimensional test case. The inset at the bottom of each column indicates the overlap of the AIMS and numerically exact wavefunctions.

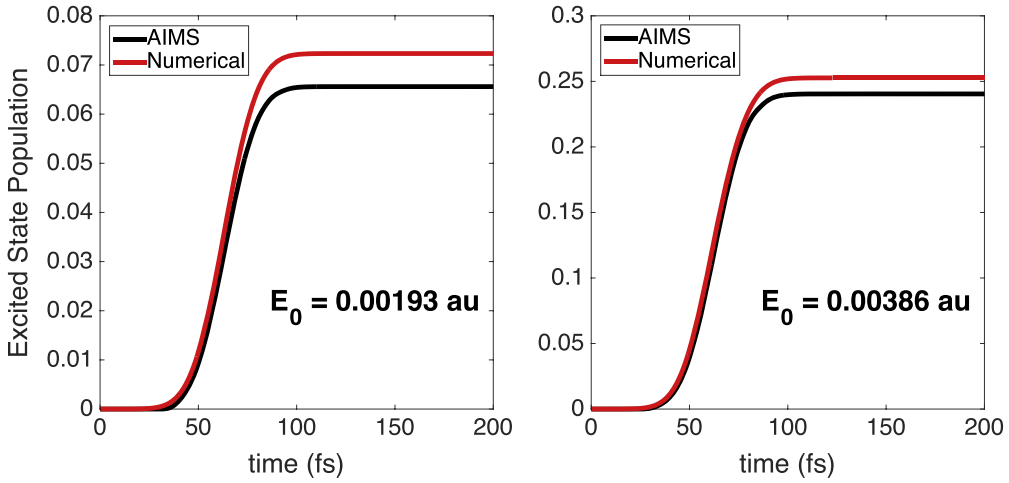

Figure 5. Population transfer during a photo-absorption process for the two-dimensional model system at two different field strengths.

different photon indices. The topology of the Floquet degeneracy is analogous to that of the CoIn as the off-diagonal dipole coupling term lifts the Floquet degeneracy just as the nonadiabatic coupling term does for the CoIn case. Therefore, each point of the QRR is an effective channel for population transfer to another state (S_0 in our case). The location where the population is transferred around this ring is important in determining the final product. Previous experimental data showed that HT suppression is at its maximum when the control field is present at relatively early times (∼50 fs); that is, when the wavepacket remains closer to the CHD side in the *g*–*h* plane [30].

In the absence of the control field, our previous simulation has shown that more than 90% of the excited state population passes through the CoIn resulting in an HT:CHD branching ratio of ≈1:1 [26]. In the presence of the control field, the population is efficiently transferred to S_0 through the LICI whenever the wavepacket in S_1 approaches the LICI; it relaxes either to CHD or HT based on the momentum and the location at which it gets transferred. Figure 8(a) shows the total transferred population through the LICI versus the delay time at which the control field pulse is applied. As we expect, the total population transferred through the LICI decreases when the control field arrives late. Our simulation shows that control via LICI is most efficient at 30–70 fs accounting for ∼10% of the total population transfer. After ∼110 fs, the external control field was not effective.

This could be explained by two effects. First, the simulated excited state lifetime is ∼108 fs [26] so there is not much population left on the excited state to be influenced by the

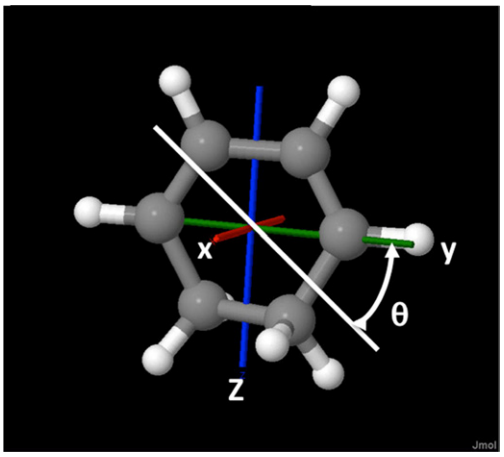

Figure 6. CHD spectroscopic axes.

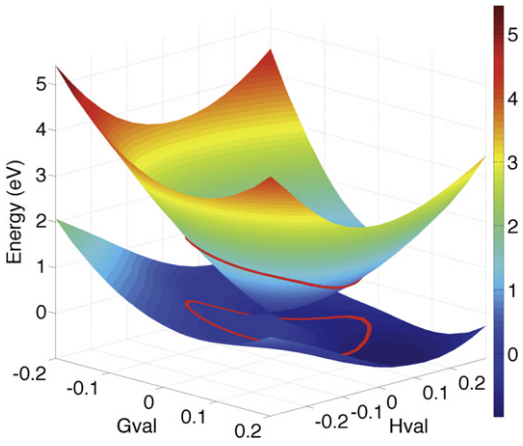

Figure 7. The S_1/S_0 CoIn topology of CHD and the 800 nm QRR in the g–h plane. The energy is relative to the S_1/S_0 CoIn energy (i.e. $E_{\mathrm{CoIn}} = 0$ eV). The QRR is an effective channel for population transfer between two states.

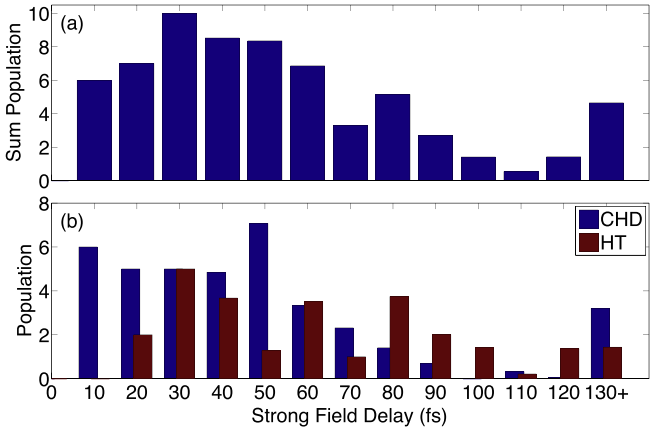

Figure 8. Results from AIMS simulations. (a) The total transferred population through the QRR is small when the control field comes in at later time delays (⩾70 fs). (b) Most of the wavepacket transferred through the QRR relaxes to the CHD (blue) than to the HT (red) when the control field control pulse comes in 0–70 fs. 130+: sum over all the population after 130 fs delay.

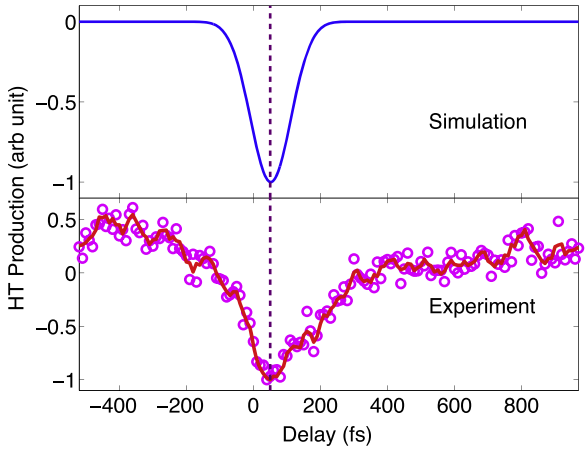

Figure 9. The comparison of the control field time delay versus HT production from the simulation (upper) and the experiment (lower). The vertical line shows the suppression of HT production is maximum at ∼50 fs for both cases.

external control field after this time. Figure 8(b) shows what fraction of the population transferred through the LICI ends up in CHD/HT. For earlier times (0–70 fs), most of the wavepacket transferred through the LICI relaxes to CHD. This means that the population, which could have relaxed to HT through CoIn in the absence of the control field, now interacts with the LICI and relaxes to the CHD ground state when the control field is applied at earlier times. This is consistent with the experiment, where HT suppression was optimized for control fields applied at ∼50–60 fs.

A second reason that the control field is ineffective after 110 fs following excitation is that the majority of the population transfer due to nonadiabatic coupling occurs around and after this time. This means that by 110 fs, most of the population is traversing the vicinity of the CoIn where the energy difference between S_0 and S_1 is very small, far from the resonant one-photon region of 1.5 eV. At much later times the AIMS results also show some fluctuation between CHD/HT. However, this effect is small since there is less population available in the excited state to interact with the LICI. The experiment reported some HT suppression at later times, but this effect may be due to the relatively long pulse width (∼70 fs) of the control field used in that work.

To simulate the experimental branching ratio time profile, we took the difference between the population which produced CHD (blue) and that which produced HT (red) in figure 8(b) and convolved the result with Gaussian functions with ∼70 fs FWHM and ∼120 fs FWHM corresponding to the experimental IR control and UV pump fields, respectively. The resulting convolved data comes close to reproducing the experimental time dependence, as shown in figure 9. The simulation successfully reproduced the direction of the branching ratio change and the location of the peak in HT suppression at ∼50 fs. The experimental suppression is less localized in delay time than the simulation. This suggests that there may be broadening effects that are not considered in the simulation. Rotational averaging would surely broaden the simulated signal and that may be part of the reason that the

Table 1. Parameters (in atomic units) used in one dimensional Morse potential model system.

	$D_{g/e}$	$b_{g/e}$	$x_{re,g/e}$	$T_{g/e}$
Ground state (g)	0.05665	0.98722	5.0386	0
Excited state (e)	0.02358	0.89747	5.7159	0.071822

computed signal is narrower than the experimental result even after convolution with the UV and IR pulse durations.

5. Conclusion

Our extension of the AIMS computational method to include an external laser field to control isomerization has successfully modeled experimental results. We have reproduced both the direction of isomerization control as well as its time profile. Also, we have shown that LICIs can efficiently shield the CoIn responsible for ring opening in CHD by intercepting and transferring population that would otherwise have passed through the original CoIn. This control scheme in CHD can control the isomerization only in one direction: HT suppression.

Since neither electronic wavefunctions nor PES shapes are modified by the field in our modified dressed-state AIMS approach, this method cannot simulate all aspects of control field control, such as dynamic Stark shifts. However despite these limitations, our simulation method provides more insight on the light–molecule interaction and that may assist future control experiments.

In our calculations, we selected the polarization of the field to be parallel to the initial transition dipole moment of the molecule to simulate an experiment where the UV pump and IR control pulses are equivalently polarized. However, the off-diagonal dipole coupling term depends strongly on the polarization of the control laser field with respect to the dipole moment of the molecule at the location of the control. We also found that the dipole moment of the molecule changes rapidly along the QRR, which suggests that the polarization of the control field would be an excellent handle for the control of the population transfer through LICI.

Our calculations also show that the final product of the control field induced transition strongly depends on the momentum of the initial wavepacket. This suggests that the shaping of the initial pump pulse along with the control laser pulse inducing transitions through LICIs will give better controllability of the CHD isomerization. The shaping of the initial wavepacket could potentially overcome the observed unidirectionality of the control in our experiment. If the wavepacket has the momentum to circumvent the original CoIn to prolong its excited state lifetime and then the control laser field is applied, more population might be transferred to the HT side via the QRR/LICI.

Acknowledgments

This research was supported by the National Science Foundation under grant number PHY-0969322. TM and HT acknowledge support by the U.S. Department of Energy, Office of Science, Office of Basic Energy Sciences, AMOS program, under contract number DE-AC02-76SF00515.

References

[1] Underwood J, Spanner M, Ivanov M, Mottershead J, Sussman B and Stolow A 2003 Switched wave packets: a route to nonperturbative quantum control *Phys. Rev. Lett.* **90** 223001

[2] Sussman B, Underwood J, Lausten R, Ivanov M and Stolow A 2006 Quantum control via the dynamic stark effect: application to switched rotational wave packets and molecular axis alignment *Phys. Rev.* A **73** 053403

[3] Halász G J, Vibók Á, Šindelka M, Moiseyev N and Cederbaum L S 2011 Conical intersections induced by light: berry phase and wavepacket dynamics *J. Phys. B: At. Mol. Opt. Phys.* **44** 175102

[4] Halász G J, Vibók Á, Šindelka M, Cederbaum L S and Moiseyev N 2012 The effect of light-induced conical intersections on the alignment of diatomic molecules *Chem. Phys.* **399** 146

[5] Halász G J, Vibók Á, Meyer H-D and Cederbaum L S 2013 Effect of light-induced conical intersection on the photodissociation dynamics of the D2 + Molecule *J. Phys. Chem.* A **117** 8528

[6] Sussman B J, Townsend D, Ivanov M Y and Stolow A 2006 Dynamic stark control of photochemical processes *Science* **314** 278

[7] Share P E, Kompa K L, Peyerimhoff S D and Van Hemert M C 1988 An MRD CI investigation of the photochemical isomerization of cyclohexadiene to hexatriene *Chem. Phys.* **120** 411

[8] Reid P J, Doig S J, Wickham S D and Mathies R A 1993 Photochemical ring-opening reactions are complete in picoseconds: a time-resolved UV resonance raman study of 1,3-cyclohexadiene *J. Am. Chem. Soc.* **115** 4754

[9] Celani P, Ottani S, Olivucci M, Bernardi F and Robb M A 1994 What happens during the picosecond lifetime of 2A1 cyclohexa-1,3-diene? A CAS-SCF Study of the cyclohexadiene/hexatriene photochemical interconversion *J. Am. Chem. Soc.* **116** 10141

[10] Pullen S, Walker L A, Donovan I , B and Sension R J 1995 Femtosecond transient absorption study of the ring-opening reaction of 1,3-cyclohexadiene *Chem. Phys. Lett.* **242** 415

[11] Fuß W, Schikarski T, Schmid W E, Trushin S and Kompa K L 1996 Ultrafast dynamics of the photochemical ring opening of 1,3-cyclohexadiene studied by multiphoton ionization *Chem. Phys. Lett.* **262** 675

[12] Trushin S A, Fuß W, Schikarski T, Schmid W E and Kompa K L 1997 Femtosecond photochemical ring opening of 1,3-cyclohexadiene studied by time-resolved intense-field ionization *J. Chem. Phys.* **106** 9386

[13] Lochbrunner S, Fuss W, Schmid W E and Kompa K-L 1998 Electronic relaxation and ground-state dynamics of 1,3-cyclohexadiene and cis-hexatriene in ethanol *J. Phys. Chem.* A **102** 9334

[14] Fuß W, Schmid W E and Trushin S A 2000 Time-resolved dissociative intense-laser field ionization for probing dynamics: Femtosecond photochemical ring opening of 1,3-cyclohexadiene *J. Chem. Phys.* **112** 8347

[15] Garavelli M, Page C S, Celani P, Olivucci M, Schmid W E, Trushin S A and Fuss W 2001 Reaction Path of a sub-200 fs photochemical electrocyclic reaction *J. Phys. Chem.* A **105** 4458
[16] Kobayashi T, Shiga M, Murakami A and Nakamura S 2007 *Ab initio* study of ultrafast photochemical ring-opening reaction of 1,3-cyclohexadiene *AIP Conf. Proc.* **963** 338
[17] Zyubina T S, Mebel A M, Hayashi M and Lin S H 2008 Theoretical study of multiphoton ionization of cyclohexadienes and unimolecular decomposition of their mono- and dications *Phys. Chem. Chem. Phys.* **10** 2321
[18] Kosma K, Trushin S A and Schmid F and W. E. 2009 Cyclohexadiene ring opening observed with 13 fs resolution: coherent oscillations confirm the reaction path *Phys. Chem. Chem. Phys.* **11** 172
[19] Schönborn J B, Sielk J and Hartke B 2010 Photochemical ring-opening of cyclohexadiene: quantum wavepacket dynamics on a global *ab initio* potential energy surface *J. Phys. Chem.* A **114** 4036
[20] Bühler C C, Minitti M P, Deb S, Bao J and Weber P M 2011 Ultrafast dynamics of 1,3-cyclohexadiene in highly excited states *J. At. Mol. Opt. Phys.* **2011** 6
[21] Arruda B C and Sension R J 2014 Ultrafast polyene dynamics: the ring opening of 1,3-cyclohexadiene derivatives *Phys. Chem. Chem. Phys.* **16** 4439
[22] Kotur M, Weinacht T, Pearson B J and Matsika S 2009 Closed-loop learning control of isomerization using shaped ultrafast laser pulses in the deep ultraviolet *J. Chem. Phys.* **130** 134311
[23] Carroll E C, White J L, Florean A C, Bucksbaum P H and Sension R J 2008 Multiphoton control of the 1,3-cyclohexadiene ring-opening reaction in the presence of competing solvent reactions *J. Phys. Chem.* A **112** 6811
[24] Hofmann A, Kurtz L and de Vivie-Riedle R 2000 Interaction of electronic structure and nuclear dynamics on the S1 reaction surface for the ring opening of cyclohexadiene *Appl. Phys.* B **71** 391
[25] Tamura H, Nanbu S, Nakamura H and Ishida T 2005 A theoretical study of cyclohexadiene/hexatriene photochemical interconversion: multireference configuration interaction potential energy surfaces and transition probabilities for the radiationless decays *Chem. Phys. Lett.* **401** 487
[26] Tao H and Martinez T J *Ab Initio* Excited State Dynamics of 1,3-cyclohexadiene Ring-opening Reactions in preparation
[27] Hofmann A and de Vivie-Riedle R 2001 Adiabatic approach for ultrafast quantum dynamics mediated by simultaneously active conical intersections *Chem. Phys. Lett.* **346** 299
[28] Carroll E C, Pearson B J, Florean A C, Bucksbaum P H and Sension R J 2006 Spectral phase effects on nonlinear resonant photochemistry of 1,3-cyclohexadiene in solution *J. Chem. Phys.* **124** 114506
[29] Geppert D and de Vivie-Riedle R 2006 Control strategies for reactive processes involving vibrationally hot product states *J. Photochem. Photobiol.* A **180** 282
[30] Kim J, Tao H, White J L, Petrović V S, Martinez T J and Bucksbaum P H 2011 Control of 1,3-cyclohexadiene photoisomerization using light-induced conical intersections *J. Phys. Chem.* A **116** 2758
[31] Halász G J, Vibók Á, Moiseyev N and Cederbaum L S 2012 Light-induced conical intersections for short and long laser pulses: floquet and rotating wave approximations versus numerical exact results *J. Phys. B: At. Mol. Opt. Phys.* **45** 135101
[32] White J L, Kim J, Petrovic V S and Bucksbaum P H 2012 Ultrafast ring opening in 1,3-cyclohexadiene investigated by simplex-based spectral unmixing *J. Chem. Phys.* **136** 054303
[33] Barbatti M 2011 Nonadiabatic dynamics with trajectory surface hopping method *Wiley Interdiscip. Rev.: Comput. Mol. Sci.* **1** 620
[34] Topaler M S, Allison T C, Schwenke D W and Truhlar D G 1998 What is the best semiclassical method for photochemical dynamics of systems with conical intersections? *J. Chem. Phys.* **109** 3321
[35] Tully J C 1990 Molecular dynamics with electronic transitions *J. Chem. Phys.* **93** 1061
[36] Tully J C 2012 Perspective: nonadiabatic dynamics theory *J. Chem. Phys.* **137** 22A301
[37] Thachuk M, Ivanov M Y and Wardlaw D M 1996 A semiclassical approach to intense-field above-threshold dissociation in the long wavelength limit *J. Chem. Phys.* **105** 4094
[38] Mitrić R, Petersen J and Bonačić-Koutecký V 2009 Laser-field-induced surface-hopping method for the simulation and control of ultrafast photodynamics *Phys. Rev.* A **79** 053416
[39] Petersen J, Mitrić R, Bonačić-Koutecký V, Wolf J-P, Roslund J and Rabitz H 2010 How shaped light discriminates nearly identical biochromophores *Phys. Rev. Lett.* **105** 073003
[40] Barbatti M, Pittner J, Pederzoli M, Werner U, Mitrić R, Bonačić-Koutecký V and Lischka H 2010 Non-adiabatic dynamics of pyrrole: dependence of deactivation mechanisms on the excitation energy *Chem. Phys.* **375** 26
[41] Mitrić R, Petersen J, Wohlgemuth M, Werner U, Bonačić-Koutecký V, Wöste L and Jortner J 2011 Time-resolved femtosecond photoelectron spectroscopy by field-induced surface hopping *J. Phys. Chem. A* **115** 3755
[42] Petersen J and Mitric R 2012 Electronic coherence within the semiclassical field-induced surface hopping method: strong field quantum control in K2 *Phys. Chem. Chem. Phys.* **14** 8299
[43] Richter M, Marquetand P, González-Vázquez J, Sola I and González L 2011 SHARC: *ab initio* molecular dynamics with surface hopping in the adiabatic representation including arbitrary couplings *J. Chem. Theory Comput.* **7** 1253
[44] Richter M, Marquetand P, González-Vázquez J, Sola I and González L 2012 Femtosecond intersystem crossing in the DNA nucleobase cytosine *J. Phys. Chem. Lett.* **3** 3090
[45] González L, Marquetand P, Richter M, González-Vázquez J and Sola I 2014 Ultrafast laser-induced processes described by *ab initio* molecular dynamics in *Ultrafast Phenomena in Molecular Sciences* vol 107 ed R de Nalda and L Bañares (Cham: Springer) p 145
[46] Marquetand P, Richter M, Gonzalez-Vazquez J, Sola I and Gonzalez L 2011 Nonadiabatic *ab initio* molecular dynamics including spin–orbit coupling and laser fields *Faraday Discuss.* **153** 261
[47] Martinez T J, Ben-Nun M and Ashkenazi G 1996 Classical/quantal method for multistate dynamics: a computational study *J. Chem. Phys.* **104** 2847
[48] Ben-Nun M and Martínez T J 2002 *Ab initio* quantum molecular dynamics *Adv. Chem. Phys.* **121** 439
[49] Ben-Nun M and Martínez T J 1998 Nonadiabatic molecular dynamics: validation of the multiple spawning method for a multidimensional problem *J. Chem. Phys.* **108** 7244
[50] Ben-Nun M, Quenneville J and Martínez T J 2000 *Ab initio* multiple spawning: photochemistry from first principles quantum molecular dynamics *J. Phys. Chem.* A **104** 5161
[51] Tao H, Levine B G and Martinez T J 2009 *Ab initio* multiple spawning dynamics using multi-state second-order perturbation theory *J. Phys. Chem.* A **113** 13656
[52] Levine B G, Coe J D, Virshup A M and Martínez T J 2008 Implementation of *ab initio* multiple spawning in the molpro quantum chemistry package *Chem. Phys.* **347** 3

[53] Mori T, Glover W J, Schuurman M S and Martinez T J 2012 Role of Rydberg states in the photochemical dynamics of ethylene *J. Phys. Chem.* A **116** 2808
[54] Ben-Nun M and Martínez T J 1998 *Ab initio* molecular dynamics study of cis–trans photoisomerization in ethylene *Chem. Phys. Lett.* **298** 57
[55] Werner H J *et al* 2012 v. MOLPRO, a package of *ab initio* programs. *v. MOLPRO, a package of ab initio programs*
[56] Breuer H P and Holthaus M 1989 Quantum phases and Landau–Zener transitions in oscillating fields *Phys. Lett.* A **140** 507
[57] Sambe H 1973 Steady states and quasienergies of a quantum-mechanical system in an oscillating field *Phys. Rev.* A **7** 2203
[58] Chu S-I and Telnov D A 2004 Beyond the floquet theorem: generalized floquet formalisms and quasienergy methods for atomic and molecular multiphoton processes in intense laser fields *Phys. Rep.* **390** 1
[59] Shirley J H 1965 Solution of the schrödinger equation with a hamiltonian periodic in time *Phys. Rev.* **138** B979
[60] Drese K and Holthaus M 1999 Floquet theory for short laser pulses *Eur. Phys. J.* D **5** 119
[61] Huang Y and Chu S-I 1994 A stationary treatment of time-dependent hamiltonian by the many-mode floquet formalism and its application to the study of effects of laser pulses in multiphoton processes *Chem. Phys. Lett.* **225** 46
[62] Korolkov M V and Schmidt B 2004 Quantum molecular dynamics driven by short and intense light pulses: towards the limits of the floquet picture *Comput. Phys. Commun.* **161** 1
[63] Guérin S and Jauslin H R 2003 Control of quantum dynamics by laser pulses: adiabatic floquet theory in *Advances in Chemical Physics* vol 125 (New York: Wiley) p 147
[64] Guérin S, Monti F, Dupont J M and Jauslin H R 1997 On the relation between cavity-dressed states, floquet states, RWA and semiclassical models *J. Phys. A: Math. Gen.* **30** 7193
[65] Ashkenazi G, Kosloff R, Ruhman S and Tal-Ezer H 1995 Newtonian propagation methods applied to the photodissociation dynamics of I3- *J. Chem. Phys.* **103** 10005
[66] Ben-Nun M and Martinez T J 2007 A continuous spawning method for nonadiabatic dynamics and validation for the zero-temperature spin boson problem *Isr. J. Chem.* **47** 75
[67] Yarkony D R 1997 Energies and derivative couplings in the vicinity of a conical intersection using degenerate perturbation theory and analytic gradient techniques. 1 *J. Phys. Chem.* A **101** 4263
[68] Yarkony D R 1996 Diabolical conical intersections *Rev. Mod. Phys.* **68** 985
[69] Yarkony D R 2001 Conical intersections: the new conventional wisdom *J. Phys. Chem.* A **105** 6277
[70] Yarkony D R 2001 Nuclear dynamics near conical intersections in the adiabatic representation: I. The effects of local topography on interstate transitions *J. Chem. Phys.* **114** 2601